
Mathematical/Statistical Research of Improved Metal Foam Heat Sink with $\text{Fe}_3\text{O}_4\text{-H}_2\text{O}$ Nanofluids

Mr. S. S. Saravanakumar¹, Mrs. K. Logasutha^{1*}, Mrs. R. Jayamani², Dr. M. Murali³, Mrs. D. Sudha⁴

¹Guest Lecturer, PG Research Department of Physics, Sethupathy Government Art's College, Ramanathapuram - 623502, Tamilnadu India. sgacsssphysics@gmail.com

^{1*}Head and Assistant Professor, Department of Mathematics, Mangayarkarasi College of Arts and Science for Women, Paravai, Madurai-625402, Tamilnadu, India. sutharaja2009@gmail.com

²Assistant Professor, PG Research Department of Chemistry, Ananda College (Affiliated to Alagappa University, Karaikudi), Devakottai, jayachem2511@gmail.com

³Associate Professor, Department of Mechanical Engineering, Kalasalingam Academy of Research and Education, m.murali@klu.ac.in

⁴Head and Assistant Professor, Department of Physics, Mangayarkarasi College of Arts and Science for Women, Paravai, Madurai-625402, Tamilnadu, India. sudhamcwphysics@gmail.com

To Cite this Article

Mr. S. S. Saravanakumar | Mrs. K. Logasutha | Mrs. R. Jayamani, "Mathematical/Statistical Research of Improved Metal Foam Heat Sink with $\text{Fe}_3\text{O}_4\text{-H}_2\text{O}$ Nanofluids" *Journal of Science and Technology*, Vol. 08, Issue 11, - July 2023, pp37-60

Article Info

Received: 29-10-2023 Revised: 08-011-2023 Accepted: 18-011-2023 Published: 28-11-2023

¹ Corresponding Author, ^{1*} Co corresponding Author

Abstract

This paper presents a numerical investigation of a proposed heat sink equipped with enhanced metal foam subjected to forced convection. The two-phase Eulerian model is employed to predict the behavior of $\text{Fe}_3\text{O}_4\text{-H}_2\text{O}$ nanofluid, to analyze heat transfer properties and entropy production. The simulation results are validated against existing data, and good agreement is achieved. The impact of pore permeability, nanoparticle size, concentration, and flow velocity on heat exchange and entropy is studied. Our results show that the application of reinforced foam enhances average Nusselt by 5.79% compared to aluminum foam, and the proposed foam application can reduce thermal entropy by 47.58% to 81.18% for Re values of 2600 and 3800, respectively. Moreover, PEC increases by 56% when the pore permeability and flow velocity are raised.

Keywords: Heat sink, electronic cooling, two-phase Eulerian model, forced convection, porous media.

1. Introduction

Microelectronic components have become indispensable in most fields, particularly media, communications, and security. As the demand for information technology grows, saving time and effort has become crucial. Nanofluids have attracted researchers' attention as one of the solutions, as they are considered the best alternative to air in terms of heat exchange and cooling efficiency [1], [2], as confirmed by several experimental studies [3]. Porous media and heat sinks are also technologies used to optimize heat transfer, and a vast field of research has attracted leading researchers [4], [5]. Dong et al. [6] studied a radial HS with triangular fins installed on a concentric cylinder and found that it reduces thermal resistance and mass compared to a reference heat sink.

Wu et al. [7] performed a numerical study to investigate how various flow and permeability characteristics affect the efficiency of HS filled with metal foams at various arrangements. E. Moghadam and J. Moghadam [8] simulated the turbulent flow of Alumina-nf in corrugated heat exchangers and found that adding 4% Al_2O_3 causes an irreversibility increase of at most 5%. To the same aim, He et al. [9] carried out a numerical analysis of geometrical parameters of ribbed pin micro-dissipators. Ming Jeng et al. [10] experimentally conducted the cooling of square-finned HS with a passage divider by forced water convection. Their results showed that the global Nu improvement is 65% compared to HS without a passage divider and packed brass beads.

Khan et al. [11] studied a hybrid nanofluid's mixed axial heat flow problem through a vertical cylinder filled with irradiated porous foam and a non-uniform heat source/dissipator. Ahmadian-Elmi et al. [12] conducted the effect of a pulsed heat pipe on the geometrical parameters of an MCHS. Yao et al. [13] examined heat transfer and irreversibility of a non-Newtonian nf in a silicon MCHS. Kavitha et al. [14] performed a computational analysis of fine-channel HS using $\text{Al}_2\text{O}_3/\text{H}_2\text{O}$ nf and distilled water as cooling fluids. The impact of a jet with a magnetic field can also yield good results in heat transfer and entropy production.

Tilehnoee and Barrio [15] analyzed heat transfer and entropy on a surface heated by a slit jet subjected to a uniform magnetic field and cooled by different nanofluids. They demonstrated that magnetic field applications could effectively reduce entropy generation. Wang et al. [16] evaluated an Oldroyd-B fluid's heat and mass transfer on a surface exposed to thermal radiation and a magnetic field. Furthermore, Tilehnoee et al. [17] considered a heated square container with 16 and 64 cylindrical solid blocks under a magnetic field to evaluate heat transfer and second law of thermodynamics.

Entropy generation effects on the flow of three different hybrid nf Carreau-ternary with a magnetic field applied to a 2D stretching area were studied by Ramzan et al. [18]. MHD-improved convection in a

metal HS filled with aluminum foam and nf was studied by Izadi et al.[19]. Mass and heat transfer effects on the bio-convective magneto-hydrodynamic peristaltic transport of Powell-Eyring nf through a curved channel with a radius-dependent magnetic field were studied by Iqbal et al.[20]. Flow and heat transfer characteristics of nf jet impaction on an MCHS with corrugated bottom were proposed and numerically studied by Cheng et al.[21]. Kushawaha et al.[22] examined a numerical study of 2D natural convection with inclined magnetic forces of Fe₃O₄-H₂O nf and Cu-H₂O non-magnetic nf inside a concentrated and exo-concentrated heated enclosure. They concluded that, at a higher value of φ %, the percentage of mass transfer reduction is 10% for Fe₃O₄-H₂O and 12% for Cu-H₂O nf. Reddy et al.[23] studied porosity effects in which radiation and viscous dissipation are present on heat and mass transfer by 2D unsteady MHD mixed convection at the standing point.

A two-phase mixing model was employed by Baghratz et al.[24] to study the role of np sedimentation on the characteristics of natural convection heat transfer within a porous channel filled with Al₂O₃-H₂O nf through time. Five rib configurations in the interrupted micro chambers of the MCHSs were analyzed by Chai and Wang[25] to identify their thermal-hydraulic performances. Several studies have been investigated to achieve the same goal[26]–[37]. Farrukh et al. [38] studied the influence of viscous dissipation on the temperature field solution of a parallel plate channel used for electronics cooling. The floating convection and heat dissipation of a saturated hybrid nf in an inclined porous pipe were studied using the Darcy-Brinkman-Forchheimer model by Reddy et al. [39]. Zhang et al. [40] applied the topological optimization method to study the geometrical design of a 2-D MCHS that cools by Al₂O₃/H₂O nf. Yang and Cao [41] proposed a multi-objective optimization of the hybrid MCHS that combines the manifold concept with secondary oblique channels.

One solution proposed to reduce heat dissipation in electronic components is using phase change materials. Krishnan et al. [42] experimentally and numerically assessed the influence of Neopentyl glycol (NPG) on PCM HS operation with heat pipe-assisted solid-solid phase transition. Mirshekar et al. [43] performed experimental research on the impact of application PCMs embedded in an open-cell Cu-foam in an HS during the heating and cooling process on different samples. Rahman et al. [44] proposed an experimental study on a nickel foam HS embedded with PCM. The literature mentioned above has highlighted various methods that have been studied and are currently used to dissipate heat from microelectronic devices, which limits their effectiveness.

The more important points mentioned in the present study are as follows:

- First, the heat sink was created with dimensions adapted to Core i9 processor sizes, which have not yet actually been considered.

- The most currently used metallic foams are aluminum or copper foams, so the idea proposed improved foam made with a combination of variable ratios of aluminum and copper to study their effectiveness in heat transfer and entropy generation.
- Improved porous foam is placed within the heat sink in opposite directions, with the two porous fins facing each other.
- Nanofluid was used instead of water to enhance heat transfer.
- The study seems comprehensive in its approach, considering various parameters that may affect heat transfer and entropy generation.

Using a two-phase Eulerian model to predict the behavior of Fe₃O₄/H₂O nf is a suitable approach, as it can provide insight into the complex interactions between the fluid and the porous foam, as it can potentially improve the performance of heat sinks used in microelectronic devices. Overall, the study seems to potentially contribute to developing more effective cooling systems for microelectronic devices and biological applications.

2. Problem description and governing equations

This study aims to simulate the proposed design of a heat sink used to cool the i9 CPU with metal foam containing aluminum and copper in different proportions to achieve more efficient foam. The properties of base metal foam used are shown in **Table 1**, with a constant metal foam porosity $\varepsilon = 0.8$. The physical depiction of studied area is illustrated in **Figure 1**. Fe₃O₄-H₂O nanofluid has been used as a coolant, the effect of the diameter of nanoparticles ($10\text{nm} \leq d_n \leq 50\text{nm}$) and their concentrations ($0.1\% \leq \varphi \leq 0.5\%$) on heat transfer and entropy generation were studied. The characteristics of the nanofluid are presented in **Table 2**. Nanofluid flow is assumed throughout the studied field to model the computational domain, and simulation was performed with steady-state, incompressible, 3D, constant thermophysical properties and two-phase (mixing and Eulerian) conditions. The radiative mode of heat transfer between the two phases is negligible. Fe₃O₄ nanoparticles and H₂O constitute two interpenetrating liquid phases. Moreover, porous foam is homogeneous, isotropic, and in thermal equilibrium with nf, with a constant porosity.

Table 1 Physical properties of the base metal foam studied

Properties	Al-foam[45]	Cu-foam	Al-Cu1 foam	Al-Cu2 foam	Al-Cu3 foam
k (W/m.K)	218	401	254.6	272.9	291.2
ρ (kg/m ³)	2719	8960	3967.2	4591.3	5215.4
Cp (J/kg.K)	871	390	774.8	726.7	678.6

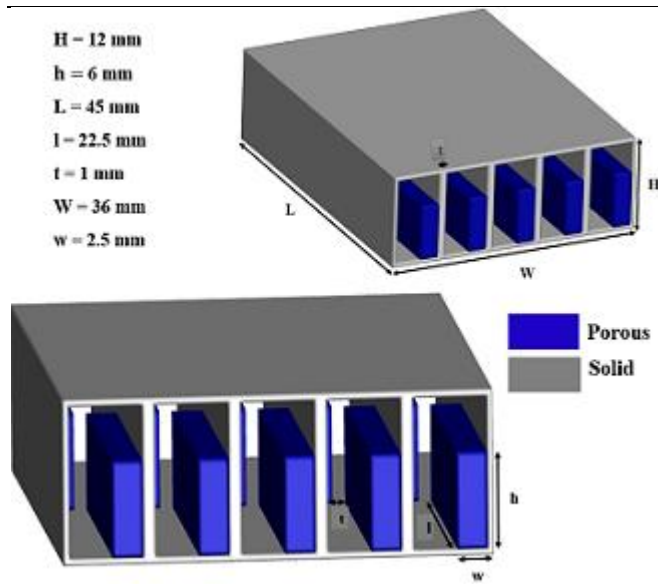


Figure 1 Schematic of heat sink, including porous fins of Al-Cu₃ foam

2.1. Eulerian multiphase method

According to the Eulerian model, the governing equations based on the above hypotheses are:

The continuity equations of the second phase are defined as follows [46]:

$$\nabla \cdot (\varphi_p \rho_p V_p) = 0 \quad (1)$$

$$\nabla \cdot (\varphi_l \rho_l V_l) = 0 \quad (2)$$

The momentum equations for the two phases are as follows :

$$\nabla \cdot (\varphi_p \rho_p V_p V_p) = -\varphi_p \nabla P + \nabla \cdot \overline{T}_p + F_{pl} \quad (3)$$

$$\nabla \cdot (\varphi_l \rho_l V_l V_l) = -\varphi_l \nabla P + \nabla \cdot \overline{T}_l + F_{lp} \quad (4)$$

The F_{pl} and F_{lp} identify the forces interacting between the two phases. The energy equation of the Eulerian phases is more approximate by:

$$\nabla \cdot (\varphi_p \rho_p h_p V_p) = \overline{T}_p \quad (5)$$

$$\nabla \cdot (\varphi_l \rho_l h_l V_l) = \overline{T}_l \quad (6)$$

Where h_p and h_l are specific enthalpies of solid and liquid phases, respectively.

2.2. k-ε Turbulence model

The k-ε standard model is a one-based on transport equations for kinetic energy of turbulence (k) and its rate of dissipation(ε) [50], which are found in the equations below:

$$\frac{\partial}{\partial t} (\rho k) + \frac{\partial}{\partial x_i} (\rho k u_i) = \frac{\partial}{\partial x_j} \left[\left(\mu + \frac{\mu_t}{\sigma_k} \right) \frac{\partial k}{\partial x_j} \right] + G_k + G_b - \rho \varepsilon - Y_m + S_k \quad (7)$$

$$\frac{\partial}{\partial t}(\rho \epsilon) + \frac{\partial}{\partial x_i}(\rho \epsilon u_i) = \frac{\partial}{\partial x_j} \left[\left(\mu + \frac{\mu_t}{\sigma_\epsilon} \right) \frac{\partial \epsilon}{\partial x_j} \right] + C_{1\epsilon} \frac{\epsilon}{k} (G_k + C_{3\epsilon} G_b) - C_{2\epsilon} \rho \frac{\epsilon^2}{k} + S_\epsilon \quad (8)$$

G_k and G_b represent the kinetic energy production of turbulence due to velocity gradients and buoyancy, respectively. Y_m is the fluctuating dilatation contribution in compressible turbulence to the global dissipation rate. $C_{1\epsilon}$, $C_{2\epsilon}$, and $C_{3\epsilon}$ are constants which $C_{1\epsilon} = 1.44$, $C_{2\epsilon} = 1.92$ [50].

σ_k and σ_ϵ are the turbulence Prandtl numbers for k and ϵ ($\sigma_k = 1$, $\sigma_\epsilon = 1.3$) [50], S_k , S_ϵ are source terms. Turbulence viscosity μ_t is determined by combining k and ϵ in the following way [50]:

$$\mu_t = \rho C_\mu \frac{k^2}{\epsilon} \quad (9) \quad \text{where } C_\mu \text{ is a constant equal } 0.09.$$

Table 2 Physical properties of Fe₃O₄-H₂O nanofluid [47]

Physical properties	ρ (kg/m ³)	Cp (J/kg.K)	k (W/m.K)	μ (Pa.s)
Water	998.1	4179	0.613	0.0013004
Fe ₃ O ₄ nanoparticle	5180	670	80	/

2.3. Thermophysical properties of nanofluid

The physical characteristics of the Fe₃O₄-H₂O nanofluid are presented in **Table 2**. The density (ρ_{nf}), dynamic viscosity (μ_{nf}), and specific heat (Cp_{nf}) of nanofluid are calculated by the following equations [47]:

$$\rho_{nf} = (1 - \phi) \rho_l + \phi \rho_p \quad (10)$$

$$\mu_{nf} = \frac{\mu_l}{(1 - \phi)^{2.5}} \quad (11)$$

$$Cp_{nf} = (1 - \phi) Cp_l + \phi Cp_p \quad (12)$$

The nanofluid thermal conductivity (k_{nf}) is calculated by [48]:

$$k_{nf} = k_l \left[\frac{k_p + 2k_l + 2\phi(k_p - k_l)}{k_p + 2k_l - \phi(k_p - k_l)} \right] \quad (13)$$

2.4. Data reduction

The average Nusselt number (Nu_{avg}) is calculated by

$$Nu = \frac{k_{nf}}{k_l} \left(\frac{\partial T}{\partial x} \times \frac{D_h}{T_{in}} \right) \quad (14)$$

$$Nu_{avg} = \frac{1}{A} \int Nu \, dA \quad (15)$$

The Reynolds number

$$Re = \frac{\rho_l V D_h}{\mu_l} \quad (16) \quad \text{where } D_h \text{ is the hydraulic diameter.}$$

Hydraulic diameter is defined as follows:

$$D_h = \frac{4A_f}{P} = 2 \frac{ab}{a+b} \quad (17) \quad \text{where } P \text{ is the perimeter (m).}$$

The equation below was employed to compute pressure drop in the working domain

$$\Delta P = P_{in} - P_{out} \quad (18)$$

Eqs estimate Performance Evaluation Criterion (PEC) and friction factor (f) are[46]:

$$PEC = \frac{Nu_{nf}/Nu_l}{\Delta P_{nf}/\Delta P_l} \quad (19)$$

$$f = \frac{\Delta P \cdot D_h}{2 \times (L \times \rho_{nf} \times V^2)} \quad (20)$$

2.5. Entropy production

The total entropy generation of the system constitutes thermal, viscous, and porous entropy components[46].

$$S_h''' = \frac{k_{nf}}{T^2} \left[\left(\frac{\partial T}{\partial x} \right)^2 + \left(\frac{\partial T}{\partial y} \right)^2 + \left(\frac{\partial T}{\partial z} \right)^2 \right] \quad (21)$$

$$S_f''' = \frac{\mu_{nf}}{T} \left\{ 2 \left[\left(\frac{\partial u}{\partial x} \right)^2 + \left(\frac{\partial v}{\partial y} \right)^2 + \left(\frac{\partial w}{\partial z} \right)^2 \right] + \left(\frac{\partial v}{\partial x} + \frac{\partial u}{\partial y} \right)^2 + \left(\frac{\partial w}{\partial y} + \frac{\partial v}{\partial z} \right)^2 + \left(\frac{\partial u}{\partial z} + \frac{\partial w}{\partial x} \right)^2 \right\} \quad (22)$$

$$S_p''' = \frac{\mu_{nf}}{T \cdot K} (u^2 + v^2 + w^2) \quad (23)$$

K is the permeability of the metal foam.

$$S_g = S_h + S_f + S_p \quad (24)$$

The system's global entropy is the integral of total entropy over the computation domain [46]

$$S_g = \int S_h''' dv + \int S_f''' dv + \int S_p''' dv \quad (25)$$

2.6. Boundary conditions

Flow problems can be numerically solved by setting the right boundary conditions (see **Figure 2**), which are as follows:

- Inlet boundary: $u = 0, v = 0, w = w_{in}$ (uniform velocity), and $T = T_{in} = 293.15K$.
- Outlet boundary: Pressure outlet $P = P_{out}$ (Atmospheric).
- Walls boundary: A no-slip condition $u = 0, v = 0, \text{ and } w = 0$.
- Heat source: $q'' = 220 \text{ kW/m}^2$.

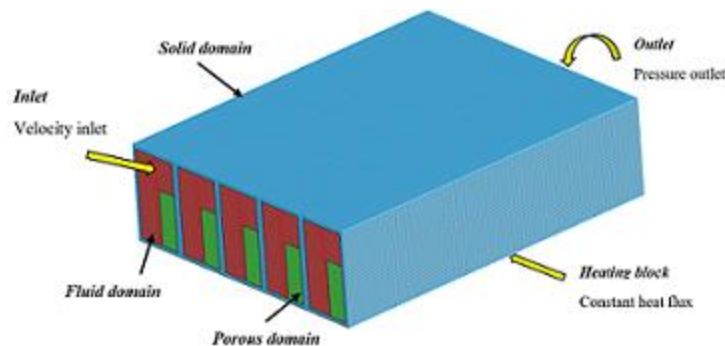


Figure 2 Mech topology and boundary conditions

3. Numerical approach, grid independence, and validation

The ANSYS-Fluent software has been used for this numerical study [50]. A simple algorithm based on finite volume method (FVM) is utilized to discretize and solve the partial differential equations (1-8). The second-order upwind schema is adopted to realize the coupling of velocity and pressure terms in momentums and energy equations. The k- ϵ standard model was selected to investigate the turbulence effect of fluid flow in the heat sink. Constant velocity inlet, atmospheric pressure outlet, and constant heat flux q'' boundary conditions (see **Figure 2**), and no-slip boundary conditions for solid-fluid, solid-porous, and fluid-porous interfaces were applied to the computational domain.

This study compares the results of the new computational model to Alhajaj et al. [49] and Ambreen et al. [46]. For validation, a five-channel HS with a length of 45 mm, width of 6 mm, and height of 12 mm have been tested. The HS bottom is filled with the opposite porous foam (properties are illustrated in **Table 1**) with dimensions $l \times w \times h$ (see **Figure 1**). A mono-phase model and laminar forced convection of water ($\varphi = 0$) are applied to metal foam ($\epsilon = 0.9$). **Figure 3** shows Nusselt's average number (Nu_{avg}) on the different flow rates (0.1, 0.15, 0.18, and 0.23), the present Nu_{avg} confirmed a satisfactory agreement with the experimental Nu_{avg} of Alhajaj et al. [49]. At 0.18 flow rate, Nu_{avg} represents a maximum deviation of 1.25%.

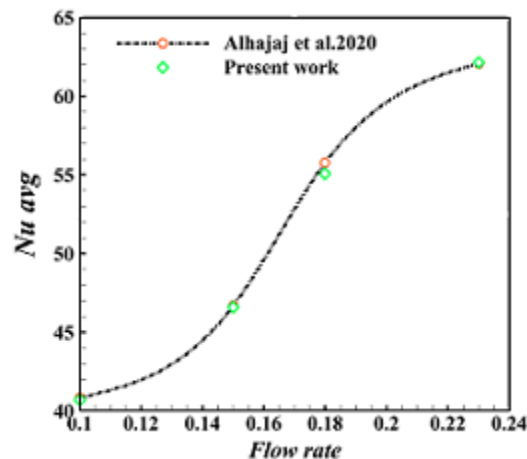


Figure 3 Comparison of Nu_{avg} of water in terms of different flow rates with the experimental results of Alhajaj et al. [49]

4. Results and discussion

4.1. Study and select the most suitable foam

In that case, the study aims to examine the effect of different mixing ratios of aluminum and copper in metallic foam on heat transfer and entropy generation. Three different foams are studied, namely Al-Cu1 (80% Al and 20% Cu), Al-Cu2 (70% Al and 30% Cu), and Al-Cu3 (60% Al and 40% Cu). The aim is to

find the optimal ratio that gives the best performance in cooling the CPU while minimizing entropy generation.

The variation of Nu_{avg} as a function of Re ($2800 \leq Re \leq 3800$) for different metal foams is shown in **Figure 4**. In agreement with the majority of previous studies [47], [42], Nu_{avg} increases with the flow acceleration. It is clear that the average Nu of Al-Cu3 foam is always the highest, followed by Al-Cu2 and then Al-Cu1, the aluminum foam gave the lowest values, with deviation estimated by 5.79% compared to Nu_{avg} of Al-Cu3 foam. This is the reason for adding the percentages of copper in the studied foam, as copper is characterized by high conductivity. The improvement of Nu_{avg} is clearer in Al-Cu3 metal foam which contains 40% copper. This amount increased the thermal conductivity of the foam used in CPU cooling, as the heat exchange coefficient h rises due to the forced convection of nf inside the foam, which leads to decreased convection/conduction ratio, therefore, an increase in Nusselt number. At $Re = 3800$, Nu_{avg} enhancement is 4.84%. As the Cu ratio increases in the foam, the Nu improves. When Re rises from 2600 to 3800, Nu_{avg} is up to 9.86% and 9.76% for Al-Cu3 and Al foam respectively.

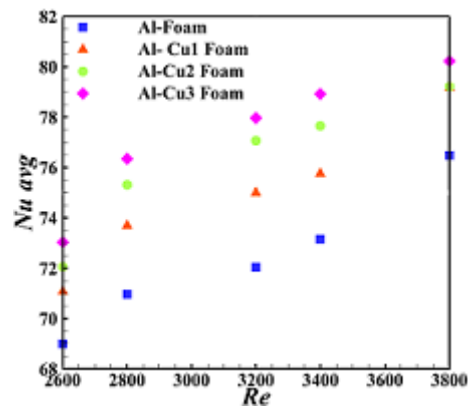


Figure 4 Average Nusselt number changes for various porous foams studied and Re number for $\phi=0.1\%$

4.2. Hydrothermal analysés

To understand the effects of nanoparticle concentration ($\phi\%$) of $Fe_3O_4-H_2O$ on thermal characteristics of the proposed HS, Nu_{avg} versus Re is indicated in **Figure 5a** for $Da=10^{-1}$, $dn=10nm$. The Nu_{avg} increases with the addition of nanoparticles and flow rate, as agreed in previous studies [46], [49]. Nusselt number represents the ratio between convection and conduction. The acceleration of nf at different concentrations inside the metal foam causes strong collisions with the surfaces of the heat sink, which decreases the convection/conduction ratio. The addition of high-speed np reduces the thickness of thermal boundary layer on the heatsink's bottom surface. All this improves heat exchange efficiency, which the

Nusselt number explains. When the volumetric concentration is raised from 0.1% to 0.5%, for $2800 \leq Re \leq 3800$, Nu ranges from 56.71% to 57.91%.

Figure 5b illustrates the evolution of pressure drops as a function of Re at different concentrations of nanoparticles in water. The rise in velocity and turbulence of Fe_3O_4 nanofluid in HS channels leads to a gradual increase in pressure drop, evident when the percentage of nanoparticles is enhanced. For a Reynolds raise from 2600 to 3800, the pressure drop is estimated at 55.34% and 56.82% for $\phi = 0.1\%$ and $\phi = 0.5\%$, respectively. The contrasting position of the porous medium and the aggravation of collisions between nf and channel surfaces, led to this high energy loss. Researchers are again trying to find the ideal position for the porous foam inside heat sinks to be effective in cooling. In this study, we supposed a different placement of the foam, as two opposing pieces in one cavity of HS.

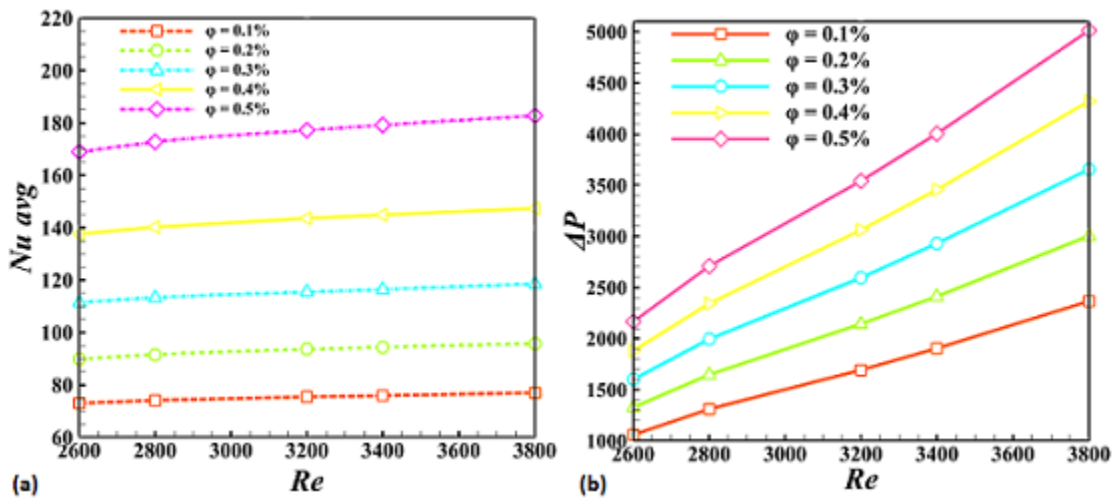


Figure 5 Changes of a) Nu_{avg} , b) ΔP with Re at different nanoparticle concentrations $\phi\%$ for $Da=10^{-1}$, $d_n=10nm$

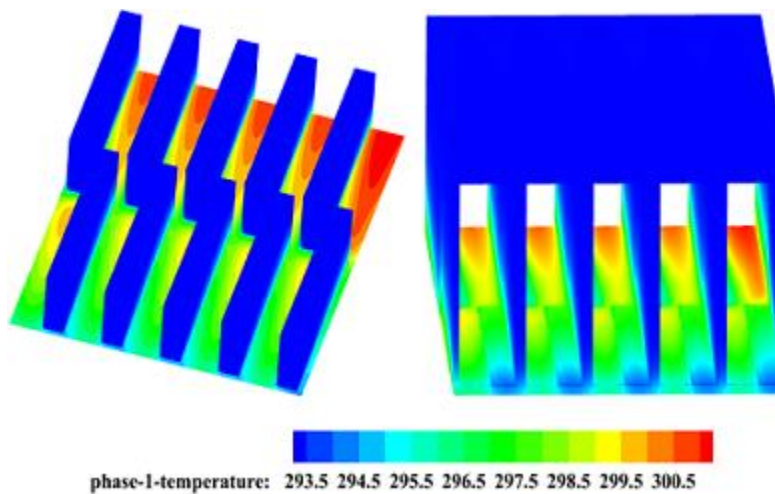


Figure 6 Effect of metal foam's position on temperature variation

Figure 6 shows temperature contour of heat sink at $Re=2800$, $\phi=0.2\%$, $Da=10^{-1}$, and $dn=10nm$. Temperature changes are at the lower basin surface and are more stable when porous media are present. The high conductivity of the Al-Cu₃ foam positioned in opposite directions in the HS channels enhanced surface exchange, and the high flow rate of Fe₃O₄-H₂O nf led to improved heat transfer, allowing the HS temperature to remain below 301 K. As shown, areas without porous foam have a higher temperature. Visually, the isotherms are denser near the heated surface, which explains the heat transfer between a heat sink and the CPU. In the porous regions, the temperature is more steady, indicating that the porous medium was able to remove excess energy inside HS due to higher conductive heat transfer, this is more evident at a higher Darcy value. Moreover, In the $z = 22.5$ mm plane, which includes the foam's opposite edges, the temperature lines near the bottom region are smooth and more ordered. The same behavior is obtained at different permeabilities. Only the length of the temperature contours increases. The Nusselt average versus Reynolds number at different permeability of metal foam (Darcy number) is presented in **Figure 7a**.

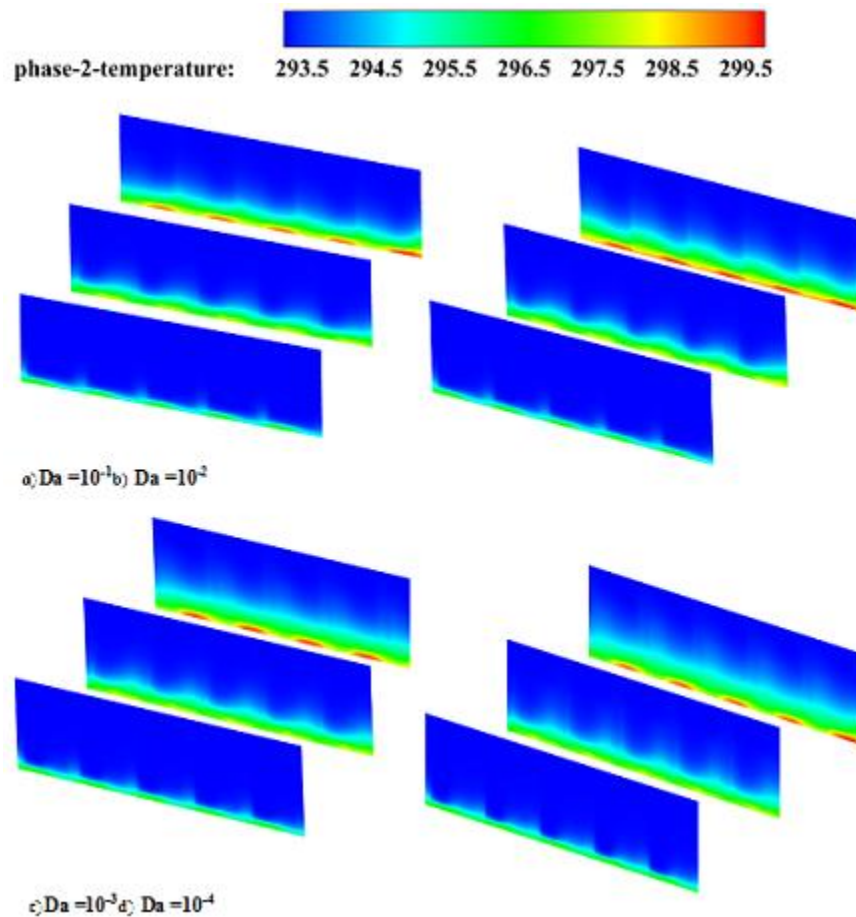


Figure 7 Heat sink temperature contours on the z -plane (5mm, 22.5mm, and 40mm) for various Da at $Re = 3200$, $\phi = 0.3\%$, $dn=20nm$

As we can see, the heat transfer rate (Nu_{avg}) increases along with increases in Re and Da numbers. This is most evident in Reynolds' high number. Regardless of nf velocity, the low permeability of porous foam makes it difficult for the liquid to pass due to the small pore size, the frequent friction between the nanoparticles, and the narrow pores. According to the results found, with all Reynolds values, raising Darcy's from 10^{-4} to 10^{-1} improves Nu_{avg} up to 23%. The maximum value of Nu_{avg} is 95.816, obtained in $Re=3800$ and $Da=10^{-1}$.

To reinforce the above results, **Figure 7b** illustrates the variation of ΔP as a function of Re at various Da . As indicated, the increase in Da and Re values results in lower pressure drop values. The reduction of pore permeability, or Da number, with the rise of nf velocity, led to an undesired increase in friction due to the limited ability of the liquid to penetrate inside the pores because of their small diameter, acting as an obstacle to the fluid flow, and resulting in increased pressure drop values. For example, at $Da=10^{-4}$ and $2800 \leq Re \leq 3800$, the amplification in ΔP is up to 55.15%.

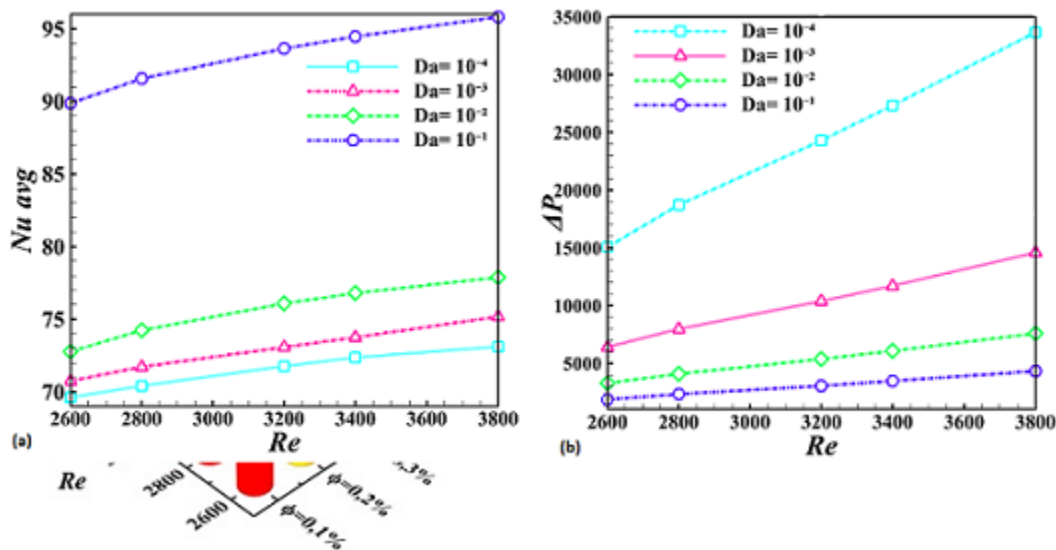


Figure 8 a and b Variation of Nu_{avg} and pressure drop in terms of Re at different Da for $\phi = 0.2\%$, $d_n=10nm$.

The increase in permeability facilitates the passage of the nanofluid into the pores and reduces friction, thus obtaining a lower pressure drop. The reduction in pressure drop is estimated at 87.53% for the same value of Re ($Re=2600$) when Da changes from 10^{-4} to 10^{-1} .

4.3. Entropy generation analysis

Investigating entropy is one of the methods to evaluate the heat exchange performance of engineering systems, especially heat sinks. Evaluation of entropy generation (entropy due to heat transfer S_H , entropy

due to viscous dissipation S_f , and entropy due to the porous medium S_p) of $Fe_3O_4-H_2O$ nanofluid in the Al-Cu3 foam with various parameters (Re , Da , $\phi\%$) are investigated in this section.

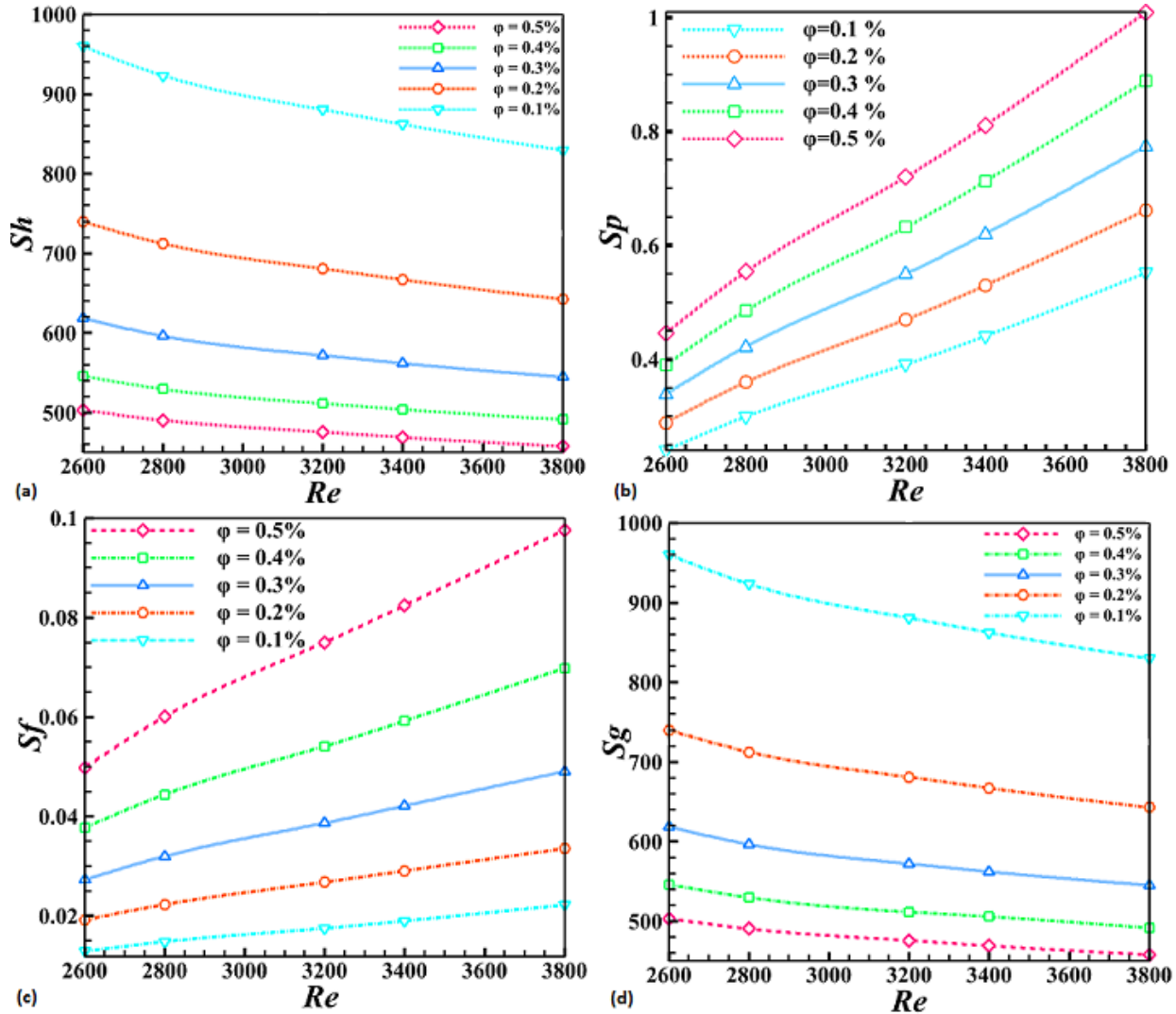


Figure 9 Effects of Re on entropy generation with different $\phi\%$ at $Da=10^{-1}$, $dn = 20nm$

Figure 9 presents the a) S_h , b) S_p , c) S_f , and d) S_g , in different Re and $\phi\%$ for $Da=10^{-1}$ and $dn = 20nm$. In agreement with general trends [31], the thermal and global entropy shows the inverse dependence on Re caused by a lower temperature gradient directly affected by forced convection. Moreover, the addition of nanoparticles leads to a significant decrease in entropy values due to the penetration of nf with high thermal conductivity into the pores, stabilizing the surface temperature. Based on equation (21), the temperature gradient strongly affects thermal entropy production, a more homogeneous medium means a lower entropy

value. As **Figure 9a** shows, when $Re = 2600$, the thermal entropy decreased at 47.58%, but the loss is more remarkable at $Re = 3800$, evaluated by 81.18%.

Figure 9b and **10c** demonstrate the variation of entropy due to porous media and viscous entropy as a function of Re with various concentrations of nanoparticles, respectively. The S_p and S_f are directly proportional to Re and $\phi\%$. The porous panels placed next to the walls of HS increase the velocity slope of nf while the velocity gradient is significant, resulting in an increase in the entropy value due to friction and the porous body. Moreover, the viscosity of nf increases with the increase of $\phi\%$ in water, leading to a rise in the frictional force. This is due to the internal force between the layers of the liquid, which is at its maximum when in contact with a solid surface. By fixing the Re number in 3200, S_p grows by 45.8% and S_f by 77.3% when the nanoparticle concentration rises from 0.1% to 0.5%. Concerning the total entropy depicted in **Figure 9d**, according to its equation (24), it is the sum of the thermal entropy, viscous, and due to porous medium. Taking into account the values of both of the latter, changes in total entropy are mainly affected by changes in thermal entropy as they dominate, and the rest is slightly influenced.

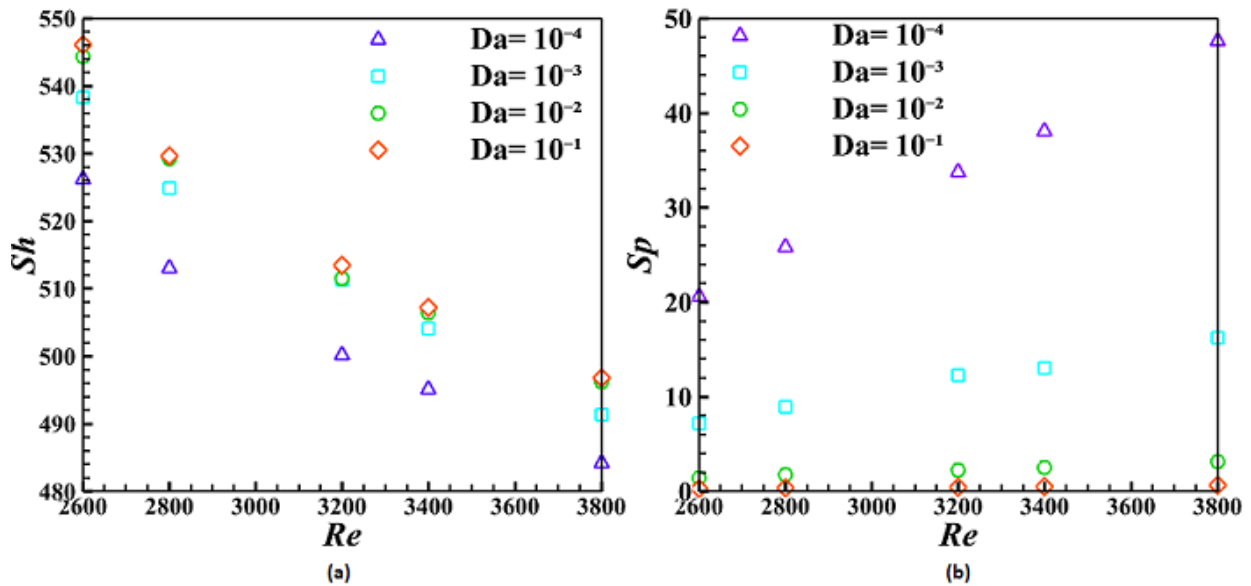


Figure 10 (a) Variations of S_h , b) S_p as a function of Re at different Da numbers

The outcomes of thermal entropy and entropy due to the porous media in metal foam HS versus flow acceleration and Da are indicated in **Figure 10**. In all Darcy values, the thermal entropy reduces with increasing nanofluid flux, while the resulting entropy of the porous medium increases with increasing Re values. As discussed previously, the enhancement of $Fe_3O_4-H_2O$ nanofluid velocity inside the reinforced metal foam leads to an acceleration of heat exchange, and the temperature gradient decreases, resulting in lower thermal entropy values. The thermal entropy values are almost identical when Darcy goes from $Da = 10^{-2}$ to $Da = 10^{-1}$. From these results, it can be said that the pore permeability has a slight effect compared

to the high nanofluid velocity. As shown in **Figure 10b**, Sp raises with Re , the increase is perceptible at lower Da values, due to the velocity enhancement, especially on the z -axis parallel to the liquid trajectory.

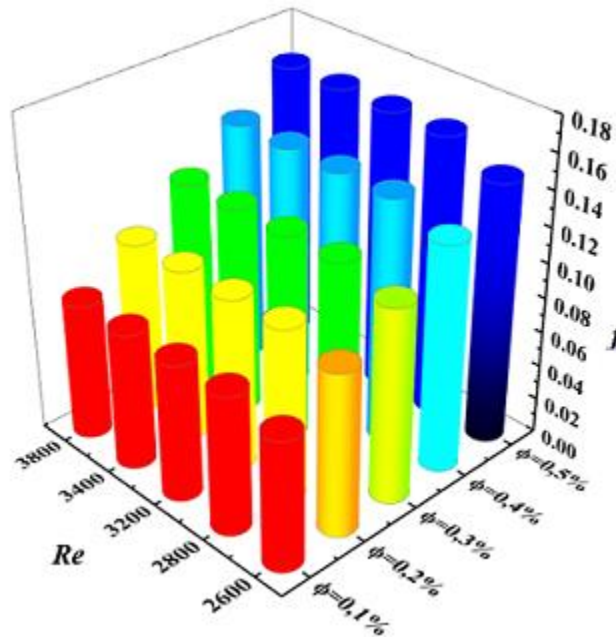


Figure 11 Friction factor as a function of Re at various concentrations of nanoparticles

The dependency of the friction factor on the flow velocity for different nanoparticle concentrations is displayed in **Figure 11**. According to equation (20), the friction factor is influenced by various parameters such as pressure drop, flow velocity, channel size, and nanofluid properties. The presence of Fe_3O_4 nanoparticles in water induces slight friction between the basic fluid layers and between the adjacent fluid layers at the heat sink walls. Hence, enhancing the concentrations of nanoparticles with higher Reynolds numbers leads to an increase in the friction coefficient. From **Figure 5**, we saw pressure drop grows with increasing coolant velocity and nanoparticle concentrations due to the high viscosity of the metal liquid ($Fe_3O_4-H_2O_{nf}$). Which has a direct influence on the growth of the friction factor at a constant value of Re , the friction factor rises to 49.6% when the concentration is changed from 0.1% to 0.5%.

5. Conclusion

To obtain an effective metal foam for cooling the Core i9 processor, this paper compared several metal foams in terms of aluminum and copper mixture ratios. After selecting the optimal foam, it was installed in a new opposite shape inside the proposed heat sink. Finite volume method (FVM) simulated the computational domain under turbulent and forced convection conditions. To increase the accuracy of the study, a two-phase Eulerian approach was used to predict the behavior of the Fe_3O_4 nanofluid in the foam. The study investigated the influence of flow velocity, nanoparticle diameter, concentration, and pore permeability on heat transfer and entropy generation. The results were presented as Nu average, pressure

drop, temperature and velocity contours, and entropy generation. The main results obtained can be summarized as follows:

- Using Al-Cu₃ foam which contains 60% aluminum and 40% copper, improves heat transfer by up to 5.79% with a constant porosity ($\varepsilon = 0.8$).
- The addition of Fe₃O₄ nanoparticles to the base fluid at different concentrations leads to an enhancement of Nu_{avg} from 56.71% to 57.91, also accompanied by an increase in pressure drop from 55.34% to 56.82% when $\varphi\%$ rises from 0.1 to 0.5, respectively.
- Increasing the nanofluid flow rate with improving pore permeability leads to a 23% enhancement in Nu_{avg} at $\varphi = 0.2\%$, $d_n = 10\text{nm}$. The placement of metal foam proposed in this study can reduce the thermal entropy by 47.58% to 81.18% for Re values of 2600 and 3800, respectively.
- Performance evaluation criteria PEC improves to 56% when the pore permeability and flow velocity are raised. Using Al-Cu₃ foam can effectively maintain the temperature of electronic components within the safe limit.

References

- [1] L. S. Sundar, K. V. Sharma, M. K. Singh, and A. C. M. Sousa, "Hybrid nanofluids preparation, thermal properties, heat transfer and friction factor – A review," *Renewable and Sustainable Energy Reviews*, vol. 68. Elsevier Ltd, pp. 185–198, Feb. 01, 2017, doi: 10.1016/j.rser.2016.09.108.
- [2] M. Habibishandiz and M. Z. Saghir, "A critical review of heat transfer enhancement methods in the presence of porous media, nanofluids, and microorganisms," *Therm. Sci. Eng. Prog.*, vol. 30, no. November 2021, p. 101267, 2022, doi: 10.1016/j.tsep.2022.101267.
- [3] Z. Tang, C. Qi, Z. Tian, and L. Chen, "Thermal management of electronic components based on new wave bio-inspired structures and nanofluids," *Int. Commun. Heat Mass Transf.*, vol. 131, no. December 2021, p. 105840, 2022, doi: 10.1016/j.icheatmasstransfer.2021.105840.
- [4] N. Zhao, L. Guo, C. Qi, T. Chen, and X. Cui, "Experimental study on thermo-hydraulic performance of nanofluids in CPU heat sink with rectangular grooves and cylindrical bugles based on exergy efficiency," *Energy Convers. Manag.*, vol. 181, no. December 2018, pp. 235–246, 2019, doi: 10.1016/j.enconman.2018.11.076.
- [5] D. Kesavan, R. Senthil Kumar, and P. Marimuthu, "Heat transfer performance of air-cooled pin-fin heatsinks: a review," *J. Therm. Anal. Calorim.*, vol. 148, no. 3, pp. 623–649, 2023, doi: 10.1007/s10973-022-11691-z.
- [6] D. Bin Kwak, H. P. Kwak, J. H. Noh, and S. J. Yook, "Optimization of the radial heat sink with a concentric cylinder and triangular fins installed on a circular base," *J. Mech. Sci. Technol.*, vol. 32, no. 1, pp. 505–512, 2018, doi: 10.1007/s12206-017-1252-4.

- [7] J. Wu *et al.*, "Thermal performance improvement of a heat-sink using metal foams for better energy storage systems," *J. Energy Storage*, vol. 60, no. December 2022, p. 106663, 2023, doi: 10.1016/j.est.2023.106663.
- [8] A. Ebrahimi-Moghadam and A. J. Moghadam, "Optimal design of geometrical parameters and flow characteristics for Al₂O₃/water nanofluid inside corrugated heat exchangers by using entropy generation minimization and genetic algorithm methods," *Appl. Therm. Eng.*, vol. 149, no. December 2018, pp. 889–898, 2019, doi: 10.1016/j.applthermaleng.2018.12.068.
- [9] Z. He, Y. Yan, and L. Zhang, "Thermal-hydraulic investigation on micro heat sinks with ribbed pin-fin arrays and single heating input: parametrical study," *J. Therm. Anal. Calorim.*, vol. 147, no. 11, pp. 6489–6505, 2022, doi: 10.1007/s10973-021-10977-y.
- [10] T. M. Jeng, S. C. Tzeng, C. W. Tseng, and C. H. Chang, "Effects of passage divider and packed brass beads on heat transfer characteristic of the pin-fin heat sink by water cooling," *Heat Mass Transf. und Stoffuebertragung*, vol. 56, no. 5, pp. 1429–1441, 2020, doi: 10.1007/s00231-019-02725-8.
- [11] U. Khan *et al.*, "Radiative mixed convective flow induced by hybrid nanofluid over a porous vertical cylinder in a porous media with irregular heat sink/source," *Case Stud. Therm. Eng.*, vol. 30, no. October 2021, p. 101711, 2022, doi: 10.1016/j.csite.2021.101711.
- [12] M. B. S. Mohammad Ahmadian-Elmi, Mohammad Reza Hajmohammadi, Seyed Salman Nourazar, Kambiz vafia, "Investigating the effect of the presence of a pulsating heat pipe on the geometrical parameters of the microchannel heat sink," *Numer. Heat Transf. Part A Appl.*, 2023, doi: <https://doi.org/10.1080/10407782.2023.2188330>.
- [13] Z. Yao *et al.*, "Numerical assessment of the impacts of non-Newtonian nanofluid and hydrophobic surfaces on conjugate heat transfer and irreversibility in a silicon microchannel heat-sink," *J. Taiwan Inst. Chem. Eng.*, vol. 142, no. December 2022, p. 104642, 2023, doi: 10.1016/j.jtice.2022.104642.
- [14] K. C. M. P.C., and A. K. C.M, "Numerical study on the performance of Al₂O₃/water nanofluids as a coolant in the fin channel heat sink for an electronic device cooling," *Mater. Today Proc.*, no. xxxx, 2023, doi: 10.1016/j.matpr.2023.02.337.
- [15] M. Hashemi-Tilehnoee and E. Palomo del Barrio, "Magneto laminar mixed convection and entropy generation analyses of an impinging slot jet of Al₂O₃-water and Novec-649," *Therm. Sci. Eng. Prog.*, vol. 36, no. August, p. 101524, 2022, doi: 10.1016/j.tsep.2022.101524.
- [16] Y. Wang *et al.*, "A three-dimensional flow of an Oldroyd-B liquid with magnetic field and radiation effects: An application of thermophoretic particle deposition," *Int. Commun. Heat Mass Transf.*, vol. 134, no. April, p. 106007, 2022, doi: 10.1016/j.icheatmasstransfer.2022.106007.

- [17] M. Hashemi-Tilehnoee, E. P. del Barrio, and S. M. Seyyedi, "Magneto-turbulent natural convection and entropy generation analyses in liquid sodium-filled cavity partially heated and cooled from sidewalls with circular blocks," *Int. Commun. Heat Mass Transf.*, vol. 134, p. 106053, 2022, doi: 10.1016/j.icheatmasstransfer.2022.106053.
- [18] M. Ramzan, F. Ali, N. Akkurt, A. Saeed, P. Kumam, and A. M. Galal, "Computational assesment of Carreau ternary hybrid nanofluid influenced by MHD flow for entropy generation," *J. Magn. Magn. Mater.*, vol. 567, no. December 2022, p. 170353, 2023, doi: 10.1016/j.jmmm.2023.170353.
- [19] A. Izadi, M. Siavashi, H. Rasam, and Q. Xiong, "MHD enhanced nanofluid mediated heat transfer in porous metal for CPU cooling," *Appl. Therm. Eng.*, vol. 168, no. December 2019, p. 114843, 2020, doi: 10.1016/j.applthermaleng.2019.114843.
- [20] J. Iqbal, F. M. Abbasi, M. Alkinidri, and H. Alahmadi, "Heat and mass transfer analysis for MHD bioconvection peristaltic motion of Powell-Eyring nanofluid with variable thermal characteristics," *Case Stud. Therm. Eng.*, vol. 43, no. December 2022, p. 102692, 2023, doi: 10.1016/j.csite.2022.102692.
- [21] J. Cheng, H. Xu, Z. Tang, and P. Zhou, "Multi-objective optimization of manifold microchannel heat sink with corrugated bottom impacted by nanofluid jet," *Int. J. Heat Mass Transf.*, vol. 201, p. 123634, 2023, doi: 10.1016/j.ijheatmasstransfer.2022.123634.
- [22] D. Kushawaha, S. Yadav, and D. K. Singh, "Magnetic field effect on double-diffusion with magnetic and non-magnetic nanofluids," *Int. J. Mech. Sci.*, vol. 191, no. September 2020, p. 106085, 2021, doi: 10.1016/j.ijmecsci.2020.106085.
- [23] V. S. R. Yanala Dharmendar Reddy, Bejawada Shankar Goud, Nagi Reddy Nalivela, "Impact of porosity on two-dimensional unsteady MHD boundary layer heat and mass transfer stagnation point flow with radiation and viscous dissipation," *Numer. Heat Transf. Part A Appl.*, 2023, doi: <https://doi.org/10.1080/10407782.2023.2198739>.
- [24] S. Baghsaz, S. Rezanejad, and M. Moghimi, "Numerical investigation of transient natural convection and entropy generation analysis in a porous cavity filled with nanofluid considering nanoparticles sedimentation," *J. Mol. Liq.*, vol. 279, pp. 327–341, 2019, doi: 10.1016/j.molliq.2019.01.117.
- [25] L. Chai and L. Wang, "Thermal-hydraulic performance of interrupted microchannel heat sinks with different rib geometries in transverse microchambers," *Int. J. Therm. Sci.*, vol. 127, no. February, pp. 201–212, 2018, doi: 10.1016/j.ijthermalsci.2018.01.029.
- [26] M. Hemmat Esfe, "Viscosity Analysis of MWCNT(25%)–ZnO(75%)/10W40 Hybrid Nanofluid; Toward a New Look at Finding Efficient Nanofluid for Heat Transfer Goals," *Arab. J. Sci. Eng.*, vol. 46, no. 6, pp. 5957–5968, 2021, doi: 10.1007/s13369-020-05091-4.

- [27] V. Saravanan and C. K. Umesh, "Numerical comparison for thermo-hydraulic performance of pin fin heat sink with micro channel pin fin heat sink," *Sadhana - Acad. Proc. Eng. Sci.*, vol. 43, no. 7, pp. 1–15, 2018, doi: 10.1007/s12046-018-0875-1.
- [28] A. A. M. Arafa, S. E. Ahmed, and M. M. Allan, "Peristaltic flow of non-homogeneous nanofluids through variable porosity and heat generating porous media with viscous dissipation: Entropy analyses," *Case Stud. Therm. Eng.*, vol. 32, no. January, p. 101882, 2022, doi: 10.1016/j.csite.2022.101882.
- [29] H. M. Maghrabie *et al.*, "Microchannel heat sinks with nanofluids for cooling electronic components: Performance enhancement, challenges, and limitations," *Therm. Sci. Eng. Prog.*, vol. 37, no. December 2022, p. 101608, 2023, doi: 10.1016/j.tsep.2022.101608.
- [30] V. R. Ram Deshmukh, "Experimental and numerical analysis of effect of combined drop-shape pin fins and plate fins type heat sink under natural convection," *Numer. Heat Transf. Part A Appl.*, no. 07/04, 2023, doi: <https://doi.org/10.1080/10407782.2023.2195128>.
- [31] M. Yang *et al.*, "A performance evaluation method based on the Pareto frontier for enhanced microchannel heat sinks," *Appl. Therm. Eng.*, vol. 212, no. April, p. 118550, 2022, doi: 10.1016/j.applthermaleng.2022.118550.
- [32] B. Buonomo, A. di Pasqua, O. Manca, S. Nappo, and S. Nardini, "Entropy generation analysis of laminar forced convection with nanofluids at pore length scale in porous structures with Kelvin cells," *Int. Commun. Heat Mass Transf.*, vol. 132, p. 105883, 2022, doi: 10.1016/j.icheatmasstransfer.2022.105883.
- [33] M. Bahiraei, N. Mazaheri, M. R. Daneshyar, and A. Mwesigye, "Two-phase simulation of irreversibilities for Ag–water nanofluid flow inside an elliptical pin-fin heat sink: Entropy generation and exergy considerations," *Powder Technol.*, vol. 409, no. April, p. 117723, 2022, doi: 10.1016/j.powtec.2022.117723.
- [34] M. Yang, M. T. Li, Y. C. Hua, W. Wang, and B. Y. Cao, "Experimental study on single-phase hybrid microchannel cooling using HFE-7100 for liquid-cooled chips," *Int. J. Heat Mass Transf.*, vol. 160, 2020, doi: 10.1016/j.ijheatmasstransfer.2020.120230.
- [35] Ya-Chu Chang, "Simulation analysis of heat transfer performance of heat sink with reduced material design," *Adv. Mech. Eng.*, vol. 12 (5) 2020, doi: 10.1177/1687814020921300.
- [36] Muhammad Jawad, Zahir Shah, Aurangzeb Khan, Saeed Islam, Hakeem Ullah, "Three-dimensional magnetohydrodynamic nanofluid thin-film flow with heat and mass transfer over an inclined porous rotating disk," *Adv. Mech. Eng.*, vol. 11 (8) 2019, doi: 10.1177/1687814019869757.
- [37] Bouziane Boudraa, Rachid Bessaïh, "Numerical investigation of heat transfer around a hot block subject to a cross-flow and an extended jet hole using ternary hybrid nanofluids," *J. Mech. Eng. Sci.*, vol. 236 2022, doi: 10.1177/09544062211049872.

- [38] M. Farrukh B, G. M. Chen, and C. P. Tso, "Viscous dissipation effect on CuO-Water nanofluid-cooled microchannel heat sinks," *Case Stud. Therm. Eng.*, vol. 26, no. November 2020, p. 101159, 2021, doi: 10.1016/j.csite.2021.101159.
- [39] N. K. Reddy, H. A. K. Swamy, M. Sankar, and B. Jang, "MHD convective flow of Ag-TiO₂ hybrid nanofluid in an inclined porous annulus with internal heat generation," *Case Stud. Therm. Eng.*, vol. 42, no. December 2022, p. 102719, 2023, doi: 10.1016/j.csite.2023.102719.
- [40] B. Zhang, J. Zhu, and L. Gao, "Topology optimization design of nanofluid-cooled microchannel heat sink with temperature-dependent fluid properties," *Appl. Therm. Eng.*, vol. 176, no. April, p. 115354, 2020, doi: 10.1016/j.applthermaleng.2020.115354.
- [41] M. Yang and B. Y. Cao, "Multi-objective optimization of a hybrid microchannel heat sink combining manifold concept with secondary channels," *Appl. Therm. Eng.*, vol. 181, no. June, p. 115592, 2020, doi: 10.1016/j.applthermaleng.2020.115592.
- [42] S. R. Akhil Krishnan, S. Sivan, V. C. Midhun, and S. R. Behera, "Experimental and numerical investigation of solid-solid phase change material assisted heat sink with integrated heat pipe for electronic cooling," *J. Energy Storage*, vol. 59, no. December 2022, p. 106494, 2023, doi: 10.1016/j.est.2022.106494.
- [43] A. Mirshekar, M. R. Goodarzi, D. Mohebbi-Kalhari, and M. H. Shafiei Mayam, "Experimental study of heat transfer enhancement using metal foam partially filled with phase change material in a heat sink," *J. Energy Storage*, vol. 60, no. August 2022, p. 106496, 2023, doi: 10.1016/j.est.2022.106496.
- [44] T. ur Rehman, T. Ambreen, H. Niyas, P. Kanti, H. M. Ali, and C. W. Park, "Experimental investigation on the performance of RT-44HC-nickel foam-based heat sinks for thermal management of electronic gadgets," *Int. J. Heat Mass Transf.*, vol. 188, p. 122591, 2022, doi: 10.1016/j.ijheatmasstransfer.2022.122591.
- [45] A. M. Bayomy, M. Z. Saghir, and T. Yousefi, "Electronic cooling using water flow in aluminum metal foam heat sink: Experimental and numerical approach," *Int. J. Therm. Sci.*, vol. 109, pp. 182–200, 2016, doi: 10.1016/j.ijthermalsci.2016.06.007.
- [46] T. Ambreen, A. Saleem, and C. W. Park, "Analysis of hydro-thermal and entropy generation characteristics of nanofluid in an aluminium foam heat sink by employing Darcy-Forchheimer-Brinkman model coupled with multiphase Eulerian model," *Appl. Therm. Eng.*, vol. 173, no. March, p. 115231, 2020, doi: 10.1016/j.applthermaleng.2020.115231.
- [47] C. Qi, K. Li, C. Li, B. Shang, and Y. Yan, "Experimental study on thermal efficiency improvement using nanofluids in heat sink with heated circular cylinder," *Int. Commun. Heat Mass Transf.*, vol. 114, p. 104589, 2020, doi: 10.1016/j.icheatmasstransfer.2020.104589.

[48] M. Zargartalebi and J. Azaiez, "Heat transfer analysis of nanofluid based microchannel heat sink," *Int. J. Heat Mass Transf.*, vol. 127, pp. 1233–1242, 2018, doi: 10.1016/j.ijheatmasstransfer.2018.07.152.

[49] Z. Alhajaj, A. M. Bayomy, M. Z. Saghir, and M. M. Rahman, "Flow of nanofluid and hybrid fluid in porous channels: Experimental and numerical approach," *Int. J. Thermofluids*, vol. 1–2, 2020, doi: 10.1016/j.ijft.2020.100016.

[50] ANSYS fluent theory guide, ANSYS, Inc, 2600 ANSYS Drive Canonsburg, PA 15317, January 2014.

Nomenclature Greek Symbols

A	Area (m ²)	μ	Viscosity (kg/m.s)
Al	Aluminum foam	ρ	Density (kg/m ³)
Cp	Specific heat (J/kg.K)	φ	Volume fraction of nanoparticles (%)
Cu	Copper foam	ϵ	Porosity
Da	Darcy number	Subscripts	
dn	Nanoparticles diameter (nm)	avg	Average
f	Friction factor	in	Inlet
H	Height (mm)	l	Liquid phase
<i>h</i>	Convective heat transfer coefficient (W/m ² K)	nf	Nanofluid
h	Height of Al-Cu ₃ foam (mm)	np	Nanoparticle
HS	Heat sink	p	Solid phase
K	Permeability (m ²)	out	Outlet
k	Heat conductivity (W/m.K)	L	Length (mm)
l	Length of Al-Cu ₃ foam (mm)	MCHS	Micro Channel Heat Sink
	MHD Magneto-hydrodynamic	Nu	Nusselt number
Nu _{avg}	Average Nusselt number	P	Pressure (Pa)
ΔP	Pressure drop (Pa)	PCM	Phase change material
PEC	Performance evaluation criteria	q''	Heat flux (W/ m ²)
T	Temperature (K)		
t	Length of space between two foams (mm)		
W	Width (mm)		
w	Width of Al-Cu ₃ foam (mm)		